# Impurity-driven transitions in frustrated quantum Ising rings

Han-Chuan Kou, Zhen-Yu Zheng, and Peng Li*

*College of Physics and Key Laboratory of High Energy Density Physics and Technology of Ministry of Education, Sichuan University, 610064 Chengdu, People's Republic of China*

(Received 14 September 2020; revised 11 January 2021; accepted 26 February 2021; published 18 March 2021)

We study the quantum phase transition driven by a point impurity in a chain seamed with ring frustration. With strong coupling and light impurity, the system is in a topological extended-kink (TEK) phase, which exhibits gapless excitations in the bulk. With strong coupling and heavy impurity, the system is in a gapped kink bound state (KBS) phase. Two-point bulk and impurity correlations are defined to characterize the two phases. In the TEK phase, both the bulk and impurity correlations are long range and factorizable so that scaling functions can be parsed. The scaling functions relies on the distance scaled by the system's size. An impurity correlation length can be extracted from the impurity correlation. In the transition from TEK to KBS, the scaling function of the bulk correlation undergoes an abrupt steplike change. Meanwhile, the impurity correlation length decreases from a divergent value to a finite one. The ground state of the TEK phase retains a relatively high value of entanglement entropy due to the absence of symmetry breaking. However, spontaneous symmetry breaking occurs in the KBS phase, which induces antiferromagnetic order in the bulk and entangled spin configuration near the impurity.

DOI: 10.1103/PhysRevE.103.032129

## I. INTRODUCTION

In the field of quantum phase transition [1], an impurity (or defect) can play important roles. For instance, it can induce remarkable bulk effects in critical or quasicritical systems [2] and pave the way to designing and fabricating quantum devices [3–5]. On the other hand, geometrical spin frustration in low dimensions can induce strong quantum fluctuations that lead to interesting phenomena [6]. Recently, the effect of ring frustrationhas attracted interest because it can provide novel quantum states [7–12]. It can produce topological extended-kink (TEK) states forming a band of gapless excitations in the bulk [13–16], which is in contrast to the usual cases of gapped symmetry-protected topological systems [17,18]. For a spin system, the simplest conditions to realize the TEK phase include a tremendous ground-state degeneracy induced by geometrical ring frustration and a source of quantum fluctuations making the kinks spread and distribute evenly in the bulk [12]. It has also been shown that a strongly interacting fermion system can fulfill the conditions and realize the effect of ring frustration [16].

It is an intriguing topic to explore the joint effect of the impurity and ring frustration. Motivated by this, we investigate the role of a point impurity in a quantum Ising chain seamed with ring frustration. In systems exhibiting ring frustration, bond defects have been introduced and studied [11,16,19]. We devote this work to the point impurity, through which we elucidate some uncovered properties in such a system, including the steplike change of the scaling function of the bulk correlation, impurity correlation length, and the absence/occurrence of spontaneous symmetry breaking. The main results in this work will not be observed in a system without ring frustration, such as a quantum Ising chain with open boundary condition [20,21].

The contents of this paper are organized as follows: In Sec. II, we construct the ground-state phase diagram basing on the rigorous solution. In Sec. III, we analyze the two-point correlation function to characterize the phases and transitions induced by the interplay between the ring frustration and impurity. In Sec. IV, we discuss the absence of symmetry breaking and entanglement entropy of the ground state in the TEK phase. Then we discuss the occurrence of spontaneous symmetry breaking in the kink bound state (KBS) phase in Sec. V. Last, we give a summary and some discussions in Sec. VI.

## II. THE MODEL AND PHASE DIAGRAM

*The model.* The model we consider reads,

$$H = J\sum_{j=1}^{N}\sigma_j^x\sigma_{j+1}^x - h\sum_{j=1}^{N-1}\sigma_j^z - \mu h\sigma_N^z, \tag{1}$$

where $\sigma_j^a (a = x, z)$ are Pauli matrices, and $\sigma_{N+j}^a = \sigma_j^a$. The geometrical ring frustration in the first term is guaranteed by the odd total number of lattice sites, $N \in$ odd, and the antiferromagnetic coupling, $J > 0$. We shall set the reference energy scale as $J = 1$, henceforth. The transverse fields are tunable so as to realize a heavy point impurity at site $N$ for $\mu > 1$ and a light one for $0 < \mu < 1$.

By the standard Jordan-Wigner transformation, $f_j^\dagger = \frac{1}{2}(\sigma_j^x + i\sigma_j^y)\prod_{l=1}^{j-1}(-\sigma_l^z)$ $(1 \leqslant j \leqslant N)$, one can find that the exact solution of the model in Eq. (1) can be mapped to the

*lipeng@scu.edu.cn

 

TABLE I. Four modes singled out in Eqs. (4) and (5) that can turn into complex modes if the corresponding root $q_i$ in Table II is a complex number.

| $\Omega_1$ | $\Omega_2$ | $\Omega_3$ | $\Omega_4$ |
|---|---|---|---|
| $\mathrm{sgn}(1-h)\omega(q_1)$ | $\omega(q_2)$ | $\omega(q_3)$ | $-\omega(q_4)$ |

proper channels of two fermion Hamiltonians [22],

$$H = P_z^- H^{\mathrm{R}} + P_z^+ H^{\mathrm{NS}}, \tag{2}$$

where the first and second terms represent the odd and even channels respectively, $P_z^{\pm} = (1 \pm \mathscr{P}_z)/2$ are projectors, $\mathscr{P}_z = \prod_{j=1}^{N}(-\sigma_j^z)$ is a parity operator, and

$$H^{\mathrm{R/NS}} = \sum_{j=1}^{N}(f_j^\dagger f_{j+1} + f_{j+1} f_j + \mathrm{H.c.}) - h\sum_{j=1}^{N-1}(2f_j^\dagger f_j - 1) - \mu h(2f_N^\dagger f_N - 1), \tag{3}$$

with the superscript R/NS meaning the "Ramond" sector or periodic boundary condition (PBC) ($f_{N+1} = f_1$) and the "Neveu-Schwarz" sector or anti-PBC ($f_{N+1} = -f_1$) respectively. We can diagonalize the fermion Hamiltonians into the form of normal modes in terms of fermion operators $\eta_q, \eta_q^\dagger$ [20,21,23,24] (the diagonalization is discussed in Appendix A),

$$H^{\mathrm{R}} = \sum_{i=1,2}\Omega_i(2\eta_i^\dagger\eta_i - 1) + \sum_q \omega(q)(2\eta_q^\dagger\eta_q - 1), \tag{4}$$

$$H^{\mathrm{NS}} = \sum_{i=3,4}\Omega_i(2\eta_i^\dagger\eta_i - 1) + \sum_q \omega(q)(2\eta_q^\dagger\eta_q - 1), \tag{5}$$

where $\Omega_i$'s are possible complex modes (listed in Table I in Appendix A), and $\sum_q$ means the sum over the rest of the quasicontinuous modes $\omega(q) = \sqrt{1 + h^2 - 2h\cos q}$.

*Ground-state phase diagram.* Let the vacua devoid of quasiparticles for $H^{\mathrm{R}}$ and $H^{\mathrm{NS}}$ be denoted by $|0^{\mathrm{R}}\rangle$ and $|0^{\mathrm{NS}}\rangle$ respectively. Then we can recover the valid states of the target Hamiltonian $H$ by picking out the valid states in the odd channel, $P_z^- H^{\mathrm{R}}$, and the even channel, $P_z^+ H^{\mathrm{NS}}$, according to Eq. (2). The ground state and the first excited state can be written as

$$|E_0^{\mathrm{R}}\rangle = \eta_1^\dagger|0^{\mathrm{R}}\rangle, \tag{6}$$

$$|E_1^{\mathrm{NS}}\rangle = \eta_3^\dagger\eta_4^\dagger|0^{\mathrm{NS}}\rangle. \tag{7}$$

For the ground state, the phase diagram is established and illustrated in Fig. 1. We get three phases: (i) TEK phase ($\mu \leqslant 1$ and $h < 1$), (ii) kink bound state (KBS) phase ($\mu > 1$ and $h < 1$), and (iii) paramagnetic (PM) phase ($h > 1$). The schematics of the ground state, the first excited state, and the lowest upper band in the transitions are depicted in Fig. 2. The TEK and KBS phases are effects of ring frustration, which are absent for a chain without ring frustration [12,21].

Because energy level crossing may occur for the first excited state in the transition between the phases, we also use $|E_{1'}^{\mathrm{NS}}\rangle$ to denote it after the level crossing. The expression for $|E_{1'}^{\mathrm{NS}}\rangle$ is the same as that in Eq. (7). For convenience, we use $|E_1^{\mathrm{NS}}\rangle$ for TEK and PM-1, and $|E_{1'}^{\mathrm{NS}}\rangle$ for KBS and PM-2, as shown in Fig. 2. And due to this energy level crossing at $\mu = 1$, we can divide the PM phase into two subphases, PM-1 and PM-2.

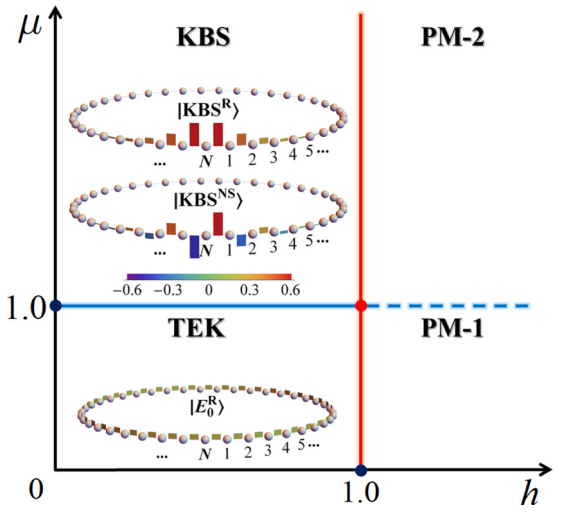


FIG. 1. Ground-state phase diagram. There are three phases: TEK, KBS, and PM. The PM phase can be divided into two subphases, PM-1 and PM-2, due to the energy level crossing of the first excited state at $\mu = 1$. The visualizations of the states in the insets are obtained by perturbative treatment on a system with $N = 41$. The parameters for $|E_0^{\mathrm{R}}\rangle$ in the TEK phase are $(h, \mu) = (0.1, 1)$, and the ones for $|\mathrm{KBS}^{\mathrm{R/NS}}\rangle$ in the KBS phase are $(h, \mu) = (0.1, 2)$.

TEK *phase.* There is no complex mode in this phase, since all $q_i$'s are real (Table II). We can divide this phase into two subphases. When $\mu = 1$, we get a translationally *symmetric*

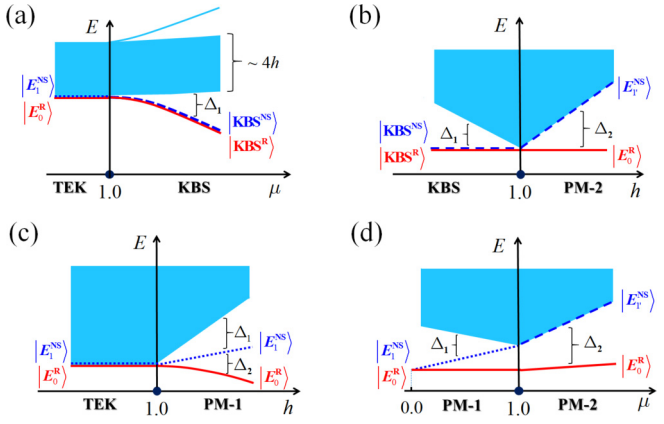


FIG. 2. Schematics of the ground state (solid red lines), the first excited state (dotted-dashed blue lines), and the lowest upper band (shaded area) in the transitions: (a) from TEK to KBS; (b) from KBS to PM-2; (c) from TEK to PM-1; (d) from PM-1 to PM-2. The schematics is obtained by Eq. (2), which leaves the energy states with valid parity. In the transitions, energy level crossing does not occur for the ground state and the first excited state in (b) and (c), but does occur for the first excited state in (a) and (d). Two kinds of energy gaps, $\Delta_2$ and $\Delta_1$, above the ground state and the first excited state are involved.

TABLE II. Asymptotic expressions of the roots $q_i$ $(i = 1, 2, 3, 4)$, when $N \gg 1$. The corresponding modes $\Omega_i$ are defined in Table I. If $q_i$ is a complex number, we may call $\Omega_i$ a complex mode. In the table, we have defined the following real parameters: $a_1 = \pi(1-h)(1-\mu)/[N(1-h)(1-\mu)+1+\mu]$, $a_3 = \pi(1-h)(1+\mu)/[N(1-h)(1+\mu)+1-\mu]$, $a_2 = \pi - a_1$, $a_4 = \pi - a_3$, $b_1 = b_3 = \ln[\sqrt{\mu^2 + h^2(1-\mu^2)^2/4} + h(1-\mu^2)/2]$, and $b_2 = b_4 = \ln[\sqrt{\mu^2 + h^2(1-\mu^2)^2/4} - h(1-\mu^2)/2]$.

| Phase | TEK | KBS | PM-1 | PM-2 |
|---|---|---|---|---|
| $q_1$ | $a_1$ | $\mathrm{i}b_1$ | $\mathrm{i}b_1$ | $a_1$ |
| $q_2$ | $a_2$ | $\pi + \mathrm{i}b_2$ | $a_2$ | $\pi + \mathrm{i}b_2$ |
| $q_3$ | $a_3$ | $\mathrm{i}b_3$ | $\mathrm{i}b_3$ | $a_3$ |
| $q_4$ | $a_4$ | $\pi + \mathrm{i}b_4$ | $a_4$ | $\pi + \mathrm{i}b_4$ |

TEK subphase that has been described in previous studies [12,16]. This phase was found to be topologically nontrivial because one can work out the winding number, $w = 1$, by the fermion Hamiltonians $H^{\mathrm{R/NS}}$ [16]. When $0 < \mu < 1$, we get a *nonsymmetric* TEK subphase because translational symmetry is gone.

There are totally $2N$ extended-kink states composing the lowest energy band of width $4h$ [see Fig. 2(a), or Fig. 9 in Appendix B). Including the ground state and the first excited state, half of them come from the odd channel, $\{\eta_1^\dagger|0^{\mathrm{R}}\rangle, \eta_2^\dagger|0^{\mathrm{R}}\rangle, \eta_q^\dagger|0^{\mathrm{R}}\rangle\}$ $(q \neq q_1, q_2)$, and half of them from the even channel, $\{\eta_3^\dagger\eta_4^\dagger|0^{\mathrm{NS}}\rangle, \eta_4^\dagger\eta_q^\dagger|0^{\mathrm{NS}}\rangle, |0^{\mathrm{NS}}\rangle\}$ $(q \neq q_3, q_4)$. Because the energy differences of adjacent levels go to zero in the order $O(1/N)$, this band becomes quasicontinuous and leads to gapless excitations in the thermodynamic limit.

A nice perturbative treatment can be applied here. The key point is to utilize the $2N$ Ising kink states (the kink is indicated by the box),

$$|j,\rightarrow\rangle = |\ldots,\leftarrow_{j-1},\boxed{\rightarrow_j,\rightarrow_{j+1}},\leftarrow_{j+2},\ldots\rangle, \tag{8}$$

$$|j,\leftarrow\rangle = |\ldots,\rightarrow_{j-1},\boxed{\leftarrow_j,\leftarrow_{j+1}},\rightarrow_{j+2},\ldots\rangle \tag{9}$$
$$(j = 1, 2, \ldots, N),$$

of the Ising Hamiltonian, $H_0 = \sum_{j=1}^{N}\sigma_j^x\sigma_{j+1}^x$, and take the restt of the Hamiltonian, $H_V = H - H_0$, as a perturbation. The degeneracy of the $2N$ Ising kink states is lifted, the ground state becomes unique, and a gapless energy band of width $4h$ comes into being. In the symmetric case ($\mu = 1$), the ground state in the perturbative picture (the lowest inset in Fig. 1) reads

$$\left|E_0^{\mathrm{R}}\right\rangle \approx \frac{1}{\sqrt{2N}}\sum_{j=1}^{N}(|j,\rightarrow\rangle + |j,\leftarrow\rangle). \tag{10}$$

The expression of it in the nonsymmetric case can be found in Appendix B. We see clearly that the kink is extended in the bulk.

KBS *phase.* In this phase, all $q_i$ $(i = 1, 2, 3, 4)$ become complex (Table II), which induces complex modes. The complex modes make both the ground state and the first excited state become KBSs. We mark them specifically as

$$|\mathrm{KBS}^{\mathrm{R}}\rangle \equiv \left|E_0^{\mathrm{R}}\right\rangle, \tag{11}$$

$$|\mathrm{KBS}^{\mathrm{NS}}\rangle \equiv \left|E_{1'}^{\mathrm{NS}}\right\rangle. \tag{12}$$

They are degenerate in the thermodynamic limit, since the energy gap between them goes to zero rapidly, $\Delta_2 \sim O(e^{-N})$. Meanwhile, a finite gap opens above them, $\Delta_1 = 2(1-h) - 2\sqrt{1+h^2-2h\cosh b_1}$ with $b_1 = \ln[h(1-\mu^2)/2 + \sqrt{\mu^2 + h^2(1-\mu^2)^2/4}]$. The number of KBSs is 2, which is a consequence of $\mathbb{Z}_2$ symmetry. We can think that there is a bulk-defect correspondence [25] between the two KBSs and the symmetric TEK phase with winding number $w = 1$.

To get a simple picture of the KBSs, we use the same perturbative treatment introduced above (see details in Appendix B). We found that the two KBSs can be expressed as

$$|\mathrm{KBS}^{\mathrm{R}}\rangle \approx \textstyle\sum_j \psi_j(|j,\rightarrow\rangle + |j,\leftarrow\rangle), \tag{13}$$

$$|\mathrm{KBS}^{\mathrm{NS}}\rangle \approx \textstyle\sum_j \chi_j(|j,\rightarrow\rangle - |j,\leftarrow\rangle), \tag{14}$$

where the coefficients are worked out as (for large enough $N \in$ odd)

$$\psi_j = \frac{\sqrt{\mu^2-1}}{2\mu} \times \begin{cases} \mu^{-j} & \left(1 \leqslant j \leqslant \frac{N-1}{2}\right), \\ \mu^{-N+j+1} & (\text{other } j), \\ 1 & (j = N-1, N), \end{cases} \tag{15}$$

$$\chi_j = \begin{cases} (-1)^j\psi_j & \left(1 \leqslant j \leqslant \frac{N-3}{2}\right), \\ (-1)^{j-1}\psi_j & (\text{other } j), \\ 0 & \left(j = \frac{N-1}{2}\right). \end{cases} \tag{16}$$

The coefficients $\psi_j$ and $\chi_j$ are depicted in the upper two insets of Fig. 1, which show clear pictures of the kink's localization near the impurity.

PM *phase.* In PM-1, the ground state is an extended state, while the first excited state shows localization behavior when the light point impurity is present. Two gaps open at the same time [Figs. 2(c) and 2(d)]. The gap from the ground state to the first excited state is $\Delta_2 = 2\sqrt{1+h^2-2h\cosh b_1}$ with $b_1 = \ln[h(1-\mu^2)/2 + \sqrt{\mu^2 + h^2(1-\mu^2)^2/4}]$. Another gap from the first excited state to the bulk band is $\Delta_1 = 2|h-1| - \Delta_2$. In PM-2, the first excited state turns into an extended state and becomes the bottom of the above band. Thus the gap $\Delta_1$ is $\sim O(1/N)$, while the gap $\Delta_2 = 2|h-1|$ remains finite [Figs. 2(b) and 2(d)].

There is a critical line $h = 1$ in the transition from TEK or KBS to PM phases. The critical behavior is similar to the one in previous studies [12,14]. In the following, we shall focus on the TEK and KBS phases.

## III. SCALING ANALYSIS OF THE TWO-POINT LONGITUDINAL CORRELATIONS OF THE TEK AND KBS PHASES

*Definitions.* The two-point longitudinal correlation function between sites $j$ and $j+r$ for the ground state $|E_0^{\mathrm{R}}\rangle$ is defined as

$$C_{j,j+r} = \langle\sigma_j^x\sigma_{j+r}^x\rangle, \tag{17}$$

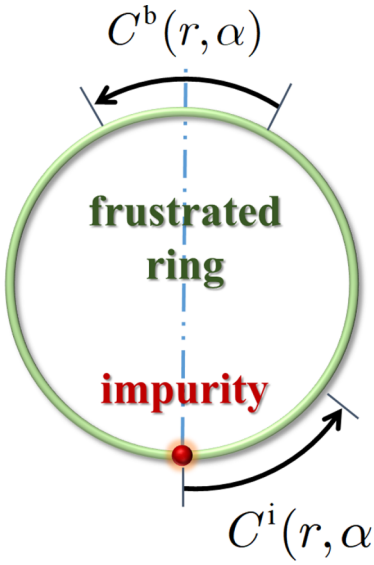


FIG. 3. Two kinds of two-point longitudinal correlation functions, $C^{\mathrm{b}}(r,\alpha)$ and $C^{\mathrm{i}}(r,\alpha)$, for bulk and impurity.

where $\langle\cdots\rangle$ means $\langle E_0^{\mathrm{R}}|\cdots|E_0^{\mathrm{R}}\rangle$. Throughout the whole paper, we only consider the longitudinal correlation function in the $x$ direction. To simplify the notation, we have dropped the superscript $xx$ and simply denoted it as $C_{j,j+r}$. By Wick's theorem, the correlation functions can be expressed in determinants, as demonstrated in Appendix C. Although translational symmetry is broken by the impurity at site $N$, there still holds a reflection symmetry (Fig. 3),

$$C_{N-j-r,N-j} = C_{j,j+r}. \tag{18}$$

We investigate two kinds of correlation functions. The first one is the *impurity correlation*, denoted by

$$C^{\mathrm{i}}(r,\alpha) \equiv C_{N,r}, \tag{19}$$

where the parameter $\alpha = r/N$ $(0 < \alpha < 1/2)$ is a distance scaled by the system's size. It measures the spin fluctuations between the impurity at site $N$ and another site $r$ in the bulk. The second one is the *bulk correlation*, denoted by

$$C^{\mathrm{b}}(r,\alpha) \equiv C_{j_0,j_0+r}, \tag{20}$$

where

$$j_0 = \frac{N-1}{2} - \left[\frac{r}{2}\right] \quad (j_0 \neq N,\ j_0 + r \neq N), \tag{21}$$

and $[\frac{r}{2}]$ means taking the integer part of $\frac{r}{2}$. For simplicity, we have chosen the two sites, $j_0$ and $j_0 + r$, to be symmetric about the impurity (Fig. 3).

As demonstrated by several exactly solvable models [14,26], finite-size scaling analysis can unravel an unusual scaling function $R(\alpha)$ due to the effect of ring frustration in the correlation function when it is a long-range one. Here, we look for the influence of the impurity.

*Bulk correlation.* We observed that the bulk correlation $C^{\mathrm{b}}(r,\alpha)$ is long range and factorizable in both the TEK and KBS phases ($h < 1$) [27],

$$C^{\mathrm{b}}(r,\alpha) = (-1)^r C^{\mathrm{b}}(r) R^{\mathrm{b}}(\alpha), \tag{22}$$

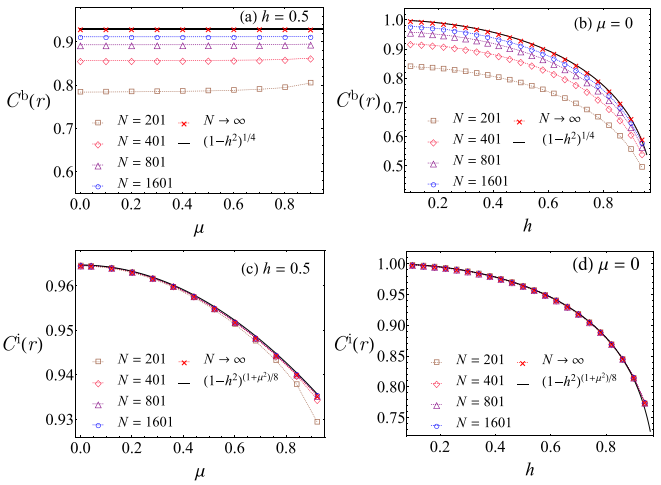


FIG. 4. Analysis of the correlations, $C^{\mathrm{b}}(r)$ and $C^{\mathrm{i}}(r)$ in Eqs. (23) and (26). The numerical data are produced by calculations on finite systems with fixed $r$ $(= 8)$ and increasing $N$ $(= 201, 401, 801, 1601)$. The numerical extrapolations to the limit $N \to \infty$ are compared with the analytical formulas in Eqs. (23) and (26). The selected parameters are $h = 0.5$ in (a) and (c), $\mu = 0$ in (b) and (d).

where

$$C^{\mathrm{b}}(r) = (1-h^2)^{\frac{1}{4}} \quad (\text{for all } \mu), \tag{23}$$

$$R^{\mathrm{b}}(\alpha) = \begin{cases} 1 - 2\alpha - \frac{2}{\pi}\sin(\alpha\pi) & (\mu < 1), \\ 1 - 2\alpha & (\mu = 1), \\ 1 & (\mu > 1). \end{cases} \tag{24}$$

We observe that the scaling function relies on the scale parameter $\alpha$ in the TEK phase and does not in the KBS phase. The former part of the correlation, $C^{\mathrm{b}}(r)$, is numerically verified and shown in Figs. 4(a) and 4(b), which fits the extrapolation of the data of finite systems quite well. The steplike scaling function $R^{\mathrm{b}}(\alpha)$ in Eq. (24) is worked out by perturbative treatment (Appendix B), and can be verified by rigorous numerical calculation and finite-size scaling analysis, as shown in Fig. 5. We label the shaded areas $A_1$ and $A_2$, which indicate the differences between the results of finite systems and that by the formula in Eq. (24). Scaling analysis in Fig. 5 shows the behaviors $A_1 \approx 1.41N^{-1}$ and $A_2 \approx 2.57N^{-0.81}$.

*Impurity correlation.* Similarly, the impurity correlation $C^{\mathrm{i}}(r,\alpha)$ is long range and factorizable in the TEK phase,

$$C^{\mathrm{i}}(r,\alpha) = (-1)^r C^{\mathrm{i}}(r) R^{\mathrm{i}}(\alpha), \tag{25}$$

where

$$C^{\mathrm{i}}(r) = (1-h^2)^{(1+\mu^2)/8} \quad (\text{for } \mu \leqslant 1), \tag{26}$$

$$R^{\mathrm{i}}(\alpha) = \begin{cases} 1 - 2\alpha + \frac{1}{\pi}\sin(2\alpha\pi) & (\mu < 1), \\ 1 - 2\alpha & (\mu = 1). \end{cases} \tag{27}$$

However, in the KBS phase ($\mu > 1$), the impurity correlation becomes a short-range one,

$$C^{\mathrm{i}}(r,\alpha) \equiv C_{N,r} \sim e^{-r/\xi_{\mathrm{i}}}, \tag{28}$$

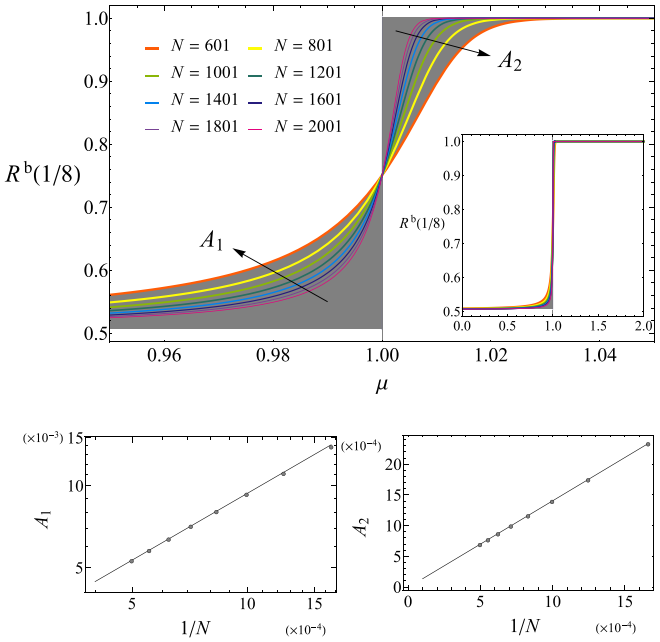





FIG. 5. Upper plot: Analysis of the scaling function $R^{\rm b}(\alpha)$ with $\alpha = 1/8$ in the transition from TEK to KBS phases, which shows the extrapolation to the limit $N \to \infty$ meets the steplike function in Eq. (24) very well. The shaded areas, $A_1$ and $A_2$, indicate the difference between the numerical data and the results by Eq. (24). The parameter $h = 0.5$ is used. Inset: the same plot in a wider scope of the parameter $\mu \in (0, 2)$. Lower left plot: Scaling analysis of $A_1$ ($\approx 1.41N^{-1}$). Lower right plot: Scaling analysis of $A_2$ ($\approx 2.57N^{-0.81}$).

where the impurity correlation length is

$$\xi_{\rm i} = \frac{1}{2\ln[\sqrt{\mu^2 + h^2(1-\mu^2)^2/4} + h(1-\mu^2)/2]}. \quad (29)$$

This formula is inferred from the result by perturbative theory (Appendix B). It can be verified numerically, since it can be defined in another way,

$$\xi_{\rm i} = \lim_{N \gg r \gg 1} \left[ \ln \left| \frac{C_{N,r}}{C_{N,r+1}} \right| \right]^{-1}. \quad (30)$$

As illustrated in Fig. 6, we observed that the data of finite systems with $r = 10, 20, 30$ and $N = 101, 201, 401, 801, 1601$ fit the formula very well. And, by scaling analysis, we found that the impurity correlation length becomes divergent when the system enters into the TEK phase, because it behaves as $\xi_{\rm i} \sim N^{\nu}$ with exponent $\nu = 1$ at the transition point $\mu = 1$ (please see the inset in Fig. 6).

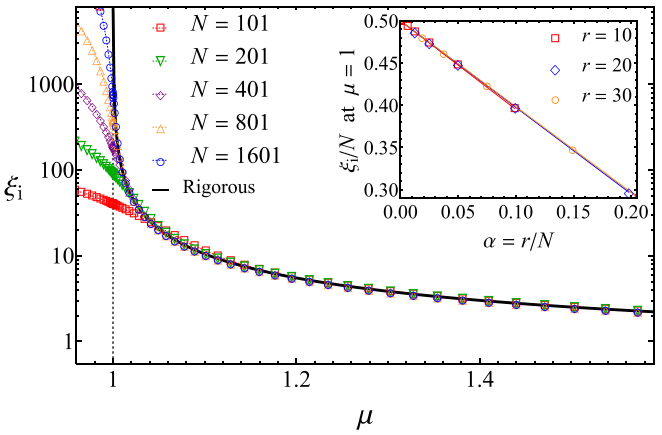


FIG. 6. Impurity correlation length $\xi_{\rm i}$ in the KBS phase. The numerical data are obtained by the formula in Eq. (30) with parameters $h = 0.5$ and varying $\mu$. The solid line denotes the rigorous formula in Eq. (29). The inset depicts scaling analysis of $\xi_{\rm i}$ at the transition point $\mu = 1$, which shows a scaling behavior, $\xi_{\rm i} \sim N^{\nu}$ with exponent $\nu = 1$.

## IV. ABSENCE OF SYMMETRY BREAKING AND ENTANGLEMENT ENTROPY OF THE GROUND STATE IN THE TEK PHASE

First, we point out the absence of symmetry breaking in the TEK phase, although it possesses long-range correlation as shown by Eqs. (23) and (24). A clear picture is provided by the perturbative theory introduced in Sec. II. We can assume that spontaneous symmetry breaking occurs for the classical Ising Hamiltonian $H_0 = \sum_{j=1}^{N} \sigma_j^x \sigma_{j+1}^x$, because the system can fall into one of the degenerate $2N$ Ising kink states with lowest energy. When the perturbation $H_V = H - H_0$ is turned on, the degeneracy is lifted and the ground state becomes nondegenerate. The ground state by the perturbative theory, Eq. (10), shows a highly entangled nature, because it contains all of the $2N$ Ising kink states with equal weight. From it, one can easily get zero value for the local magnetic order parameter $m_x = \langle \sigma_j^x \rangle = 0$ for any site $j$. Moreover, it is not hard to prove this result for the rigorous ground state in Eq. (6). Thus the symmetry breaking in $H_0$ is absent now. Now that the ground state in the TEK phase exhibits an entangled nature, we can use the entanglement entropy to characterize it rigorously. Following the standard procedure [28], we divide the system into two half parts: part A containing sites from $\frac{N-1}{2}$ to $N-1$ and part B containing the rest. we can obtain the reduced density matrix by tracing over the degrees of freedom of one of the subsystem, $\rho^{\rm A/B} = {\rm tr}_{\rm B/A}(\rho)$ with $\rho = |E_0^{\rm R}\rangle\langle E_0^{\rm R}|$. Then the block entanglement entropy $S$ between the two subsystems is obtained by $S = -{\rm tr}(\rho^{\rm A} \log_2 \rho^{\rm A}) = -{\rm tr}(\rho^{\rm B} \log_2 \rho^{\rm B})$. The numerical results are illustrated in Fig. 7. We observe that the value of $S$ is always higher than 2 in the TEK phase and turns down at the transition point $\mu = 1$. For comparison, the result for the well-known Greenberger-Horne-Zeilinger (GHZ) state is 1, and the one for the Affleck-Kennedy-Lieb-Tasaki (AKLT) model is 2 [29].

## V. SYMMETRY BREAKING IN THE KBS PHASE

Now, we show that the $\mathscr{P}_z$ symmetry can be broken in the KBS phase. We can display this phenomenon by defining two states,

$$|\pm\rangle = \frac{1}{\sqrt{2}}(|{\rm KBS}^{\rm R}\rangle \pm |{\rm KBS}^{\rm NS}\rangle), \quad (31)$$

whose $\mathscr{P}_z$ symmetry is broken. Then the occurrence of spontaneous symmetry breaking can be obviously seen in the framework of perturbative theory. By substituting Eqs. (13) and (14) into Eq. (31), we can write the states $|\pm\rangle$ in the

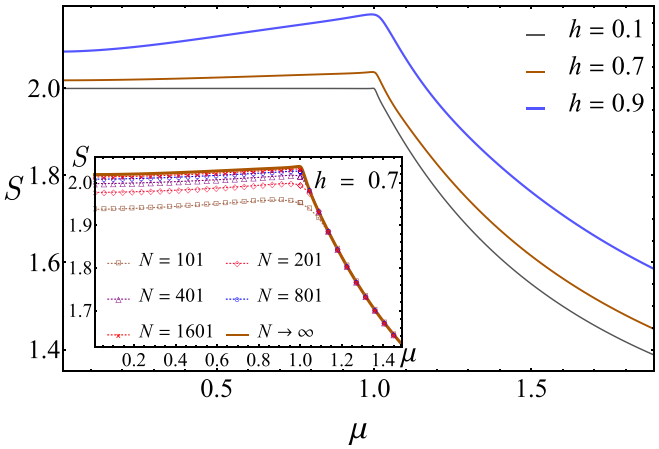


FIG. 7. Entanglement entropy $S$ of the ground state in the TEK and KBS phases. The selected parameters are $h = 0.1, 0.7, 0.9$ and varying $\mu$. The inset shows the scaling analysis for the case of $h = 0.7$. Please see the text for more details.

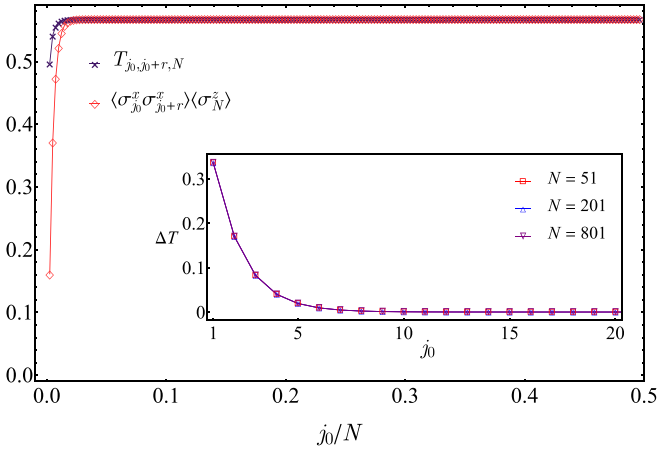


FIG. 8. Three-site correlation function $T_{j_0,j_0+r,N}$ and the product $\langle\sigma^x_{j_0}\sigma^x_{j_0+r}\rangle\langle\sigma^z_N\rangle$, for a system with size $N = 401$ and parameters $h = 0.1$ and $\mu = 1.5$. When $j_0$ is far away from the impurity, we have $T_{j_0,j_0+r,N} \approx \langle\sigma^x_{j_0}\sigma^x_{j_0+r}\rangle\langle\sigma^z_N\rangle$, which means $T_{j_0,j_0+r,N}$ is factorizable in the thermodynamic limit. However, it cannot be factorized when site $j_0$ is near the impurity, which is reflected by the difference, $\Delta T = T_{j_0,j_0+r,N} - \langle\sigma^x_{j_0}\sigma^x_{j_0+r}\rangle\langle\sigma^z_N\rangle$, as shown in the inset.

approximate form,

$$|\pm\rangle \approx \sum_{m=1,2,3,\cdots} \lambda_m |\text{imp}\rangle_m \otimes |\text{bulk}, \pm\rangle_m, \tag{32}$$

where $\lambda_m = \sqrt{\mu^2 - 1}/(\sqrt{2}\mu^m)$ is the weight of each component labeled by $m$, $|\text{imp}\rangle_m$ denotes the entangled impurity part of the component that can be written as

$$|\text{imp}\rangle_1 = |\rightarrow_N\rangle + |\leftarrow_N\rangle, \tag{33}$$

$$|\text{imp}\rangle_2 = |\leftarrow_{N-1}, \rightarrow_N, \leftarrow_1\rangle + |\rightarrow_{N-1}, \leftarrow_N, \rightarrow_1\rangle, \tag{34}$$

$$\begin{aligned}|\text{imp}\rangle_3 = {} & |\rightarrow_{N-2}, \leftarrow_{N-1}, \rightarrow_N, \leftarrow_1, \rightarrow_2\rangle \\ & + |\leftarrow_{N-2}, \rightarrow_{N-1}, \leftarrow_N, \rightarrow_1, \leftarrow_2\rangle, \end{aligned} \tag{35}$$

$$\vdots$$

and $|\text{bulk}, \pm\rangle_m$ denotes the antiferromagnetic bulk part of the component. If $m \in$ odd, they read

$$|\text{bulk}, +\rangle_m = |\rightarrow_m, \leftarrow_{m+1}, \ldots, \leftarrow_{N-m}\rangle, \tag{36}$$

$$|\text{bulk}, -\rangle_m = |\leftarrow_m, \rightarrow_{m+1}, \ldots, \rightarrow_{N-m}\rangle, \tag{37}$$

while if $m \in$ even, they swap the expressions. Because $\lambda_m$ decreases rapidly with $m$ increasing, the entangled impurity parts, $|\text{imp}\rangle_m$, show almost the same localization behavior in the broken states $|\pm\rangle$ as that in $|\text{KBS}^{\text{R/NS}}\rangle$.

To observe this symmetry breaking by rigorous calculation, we define a special three-point correlation function among sites $j_0$, $j_0 + r$, and $N$ for the ground state $|E_0^{\text{R}}\rangle$,

$$T_{j_0,j_0+r,N} = \langle\sigma^x_{j_0}\sigma^x_{j_0+r}\sigma^z_N\rangle, \tag{38}$$

in which $j_0$ is defined in Eq. (21). $T_{j_0,j_0+r,N}$ can be expressed in determinants (Appendix C) and can be evaluated efficiently for quite large systems. In the TEK phase, it gives zero value. In the KBS phase, we demonstrate that it is an adequate quantity for observing the symmetry breaking of the KBS phase. The numerical result is illustrated in Fig. 8. We see that $T_{j_0,j_0+r,N}$ can be factorized into a product of a two-point bulk correlation and a one-point impurity average,

$$\langle\sigma^x_{j_0}\sigma^x_{j_0+r}\sigma^z_N\rangle \approx \langle\sigma^x_{j_0}\sigma^x_{j_0+r}\rangle\langle\sigma^z_N\rangle, \tag{39}$$

when both $N$ and $j_0$ are large enough. This signifies a symmetry breaking in the bulk, because the two-point bulk correlation is a long-range one, $\langle\sigma^x_{j_0}\sigma^x_{j_0+r}\rangle \equiv C_{j_0,j_0+r} = (1 - h^2)^{\frac{1}{4}}$. Notice that we have $R^{\text{b}}(\alpha) = 1$ now, according to Eq. (24). Thus we can define the order parameter for the bulk in the conventional way [30] and get

$$m_x = \langle\sigma^x_{j_0}\rangle = \sqrt{|C_{j_0,j_0+r}|} = (1 - h^2)^{\frac{1}{8}} \ (j_0 \gg 1). \tag{40}$$

As a bonus, $T_{j_0,j_0+r,N}$ can also reflect the localized and entangled part of the ground state near the impurity ($j_0 \gtrsim 1$). As shown in the inset of Fig. 8, we observe that it cannot be factorized for small $j_0$ and the difference $\Delta T = T_{j_0,j_0+r,N} - \langle\sigma^x_{j_0}\sigma^x_{j_0+r}\rangle\langle\sigma^z_N\rangle$ is robust against the change of the system's size near the impurity.

## VI. SUMMARY AND DISCUSSION

In summary, we have constructed the ground-state phase diagram of the frustrated quantum Ising chain in the presence of a point impurity. The impurity can tune the system to depart from the symmetric TEK phase. Light impurity induces a gapless nonsymmetric TEK phase and heavy impurity induces a KBS phase. Both phases are characterized by two-point longitudinal correlations. It was demonstrated that the correlations can be factorized when they are long-range ones. The scaling function of the bulk correlation is shown to undergo a steplike change in the transition between the two phases. The absence of spontaneous symmetry breaking in the TEK phase is stressed and entanglement entropy is calculated to reflect the entangled nature of the ground state. In contrast, spontaneous symmetry breaking occurs in the KBS phase, which induces antiferromagnetic order in the bulk and entangled spin configuration near the impurity.

Next, we discuss some important issues. First, PBC is of great theoretical and experimental interest. Theoretically, it can produce fascinating phase transitions and critical phenomena [31–35]. Experimentally, there ha been much impressive progress in designing and fabricating quantum devices with ring structure to achieve potential applications [36,37]. In our model, PBC is indispensable, because it maintains the geometrical ring frustration and leads to the TEK and KBS phases. In the same parameter region ($h < 1$), one would get an usual antiferromagnetically ordered phase when there is no ring frustration, e.g., the periodic chain with $N \in$ even or the open chain [21]. Our work shows that the effect of ring frustration can be exploited to realize exotic quantum phases and transitions. Second, the gapless TEK phase is distinct from the critical models with gapless excitations in the literature [35,38], since the entanglement entropy does not diverge here. To maintain the effect of ring frustration, we did not cut the ring and resorted to the bulk-defect correspondence instead of the bulk-boundary correspondence as discussed in Sec. II, which indicates that the TEK phase with gapless bulk excitations is unconventional. In fact, the gapless TEK phase does not belong to the typical categories of gapped phases with symmetry-protected topological order or symmetry-breaking order [18]. So how to categorize it remains an open question. Finally, we must consider interaction terms in a pure fermion system to realize the effect of ring frustration [16]. Thus the frustrated spin model in this work has an interacting nature. It would be very interesting to explore similar phenomena in other relevant systems in which ring frustration can play an important role.


## ACKNOWLEDGMENTS

We thank Yan He for useful discussions. This work is supported by the NSFC under Grant No. 11074177.


## APPENDIX A: DIAGONALIZATION OF $H^{\mathrm{R/NS}}$

Here, we mainly explain the diagonalization of $H^{\mathrm{R}}$ since the procedure for $H^{\mathrm{NS}}$ is almost the same. $H^{\mathrm{R}}$ can be rewritten as [20,21,23,24]

$$H^{\mathrm{R}} = \sum_{i,j}\left[f_i^\dagger A_{ij} f_j + \frac{1}{2}(f_i^\dagger B_{ij} f_j^\dagger + \mathrm{H.c.})\right]. \tag{A1}$$

The real matrices $A$ and $B$ are symmetric and antisymmetric respectively, and their elements are given by $A_{i,j} = J(\delta_{i,j+1} + \delta_{i+1,j}) + 2h[(1-\mu)\delta_{i,N} - 1] + J(\delta_{1,N} + \delta_{N,1})$ and $B_{i,j} = J(\delta_{i,j+1} - \delta_{i+1,j}) - J(\delta_{1,N} - \delta_{N,1})$. We try to find a linear transformation

$$\begin{aligned}\eta_q &= \sum_j (g_{q,j} f_j + h_{q,j} f_j^\dagger),\\ \eta_q^\dagger &= \sum_j (g_{q,j} f_j^\dagger + h_{q,j} f_j)\end{aligned} \tag{A2}$$

with canonical coefficients $g_{q,j}$ and $h_{q,j}$, so that we can transform the Hamiltonian into a diagonalized form,

$$H^{\mathrm{R}} = \sum_{i=1,2} \Omega_i (2\eta_i^\dagger \eta_i - 1) + \sum_q \omega(q)(2\eta_q^\dagger \eta_q - 1), \tag{A3}$$

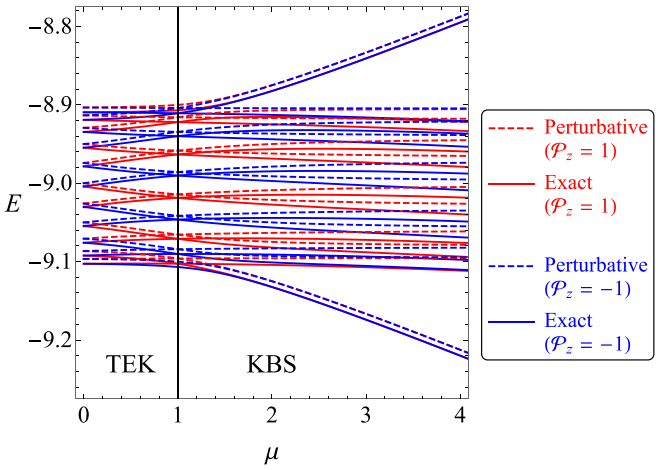


FIG. 9. Comparison of the low-energy levels by perturbative theory (dashed lines) and exact solution (solid lines) in the TEK and KBS phases for $N = 11$ and $h = 0.05$. The red and blue lines are for parities $\mathscr{P}_z = 1$ and $-1$ respectively. With $N$ increasing, the energy levels in the middle become quasicontinuous.

where $\Omega_1$ and $\Omega_2$ are defined in Table I, and $q$ in $\sum_q$ runs over the rest of the quasicontinuous modes, $\omega(q) = 2\sqrt{1+h^2-2h\cos q}$.

To work out the values of $q$, we introduce two matrices: $\Phi$ with elements $\phi_{q,j} = g_{q,j} + h_{q,j}$ and $\Psi$ with elements $\psi_{q,j} = g_{q,j} - h_{q,j}$. This leads to the eigenvalue problem

$$\begin{aligned}\omega^2\Phi &= \Phi(A-B)(A+B),\\ \omega^2\Psi &= \Psi(A+B)(A-B),\end{aligned}$$

where $\omega = \mathrm{diag}(\ldots, \omega(q), \ldots)$ is a diagonal matrix that consists of eigenvalues. Then, following the standard procedure described in Refs. [23,24,39], we arrive at the equation

$$\begin{aligned}&2\mathscr{P}_z\mu \sin q + h(\mu^2 - 1)\sin Nq\\ &\quad + \sin(N+1)q - \mu^2 \sin(N-1)q = 0\end{aligned} \tag{A4}$$

with $\mathscr{P}_z = -1$. All independent $q$ (including $q_1$ and $q_2$) are roots of this equation. Notice that Eq. (A4) has an extra boundary term, $2\mathscr{P}_z\mu \sin q$, compared with the free open boundary case [20]. It can be solved numerically. When $N \in$ odd is large enough, we can work out the asymptotic expressions of the roots $q_i$ $(i = 1, 2, 3, 4)$, as shown in Table II, in which the phases are described in Sec. II of the main text. $\Omega_1$ and $\Omega_2$ defined in Table I can become complex modes when the corresponding roots denoted by $q_1 = a_1 + ib_1$ and $q_2 = a_2 + ib_2$ are complex numbers as shown in Table II. We have observed that the roots $q_1$ and $q_2$ change continuously from real numbers to complex ones in the transitions. For instance, $q_1 : a_1 \to 0 \to ib_1$ and $q_2 : a_2 \to \pi \to \pi + ib_2$.

Likewise we can transform $H^{\mathrm{NS}}$ to

$$H^{\mathrm{NS}} = \sum_{i=3,4} \Omega_i (2\eta_i^\dagger \eta_i - 1) + \sum_q \omega(q)(2\eta_q^\dagger \eta_q - 1). \tag{A5}$$

where $\Omega_3$ and $\Omega_4$ are defined in Table I. They can become complex modes when the roots denoted by $q_3 = a_3 + ib_3$ and $q_4 = a_4 + ib_4$ are complex numbers as shown in Table II. All independent $q$ (including $q_3$ and $q_4$) are roots of Eq. (A4)

with $\mathscr{P}_z = 1$. We have also observed that the roots $q_3$ and $q_4$ change continuously from real numbers to complex ones in the transitions.

## APPENDIX B: PERTURBATIVE THEORY FOR THE TEK AND KBS PHASES

The perturbative theory is carried out in the subspace composed of the one-kink Ising states in Eqs. (8) and (9), which are also eigenstates of the main Hamiltonian $H_0 = \sum_{j=1}^{N} \sigma_j^x \sigma_{j+1}^x$. As a perturbation ($h \ll 1$), the transverse term $H_V = H - H_0$ does not commute with $H_0$, so we can get approximate eigenstates by diagonalizing it in this subspace. Because of the commutator $[\mathscr{P}_z, H] = 0$, we introduce another set of states with good quantum number of $\mathscr{P}_z$, $|j,\uparrow\rangle = (|j,\rightarrow\rangle + |j,\leftarrow\rangle)/\sqrt{2}$ and $|j,\downarrow\rangle = (|j,\rightarrow\rangle - |j,\leftarrow\rangle)/\sqrt{2}$, so as to get the effective Hamiltonian,

$$\begin{aligned} H_{\text{eff}} = \sum_{j=1}^{N} [&(2-N)(|j,\uparrow\rangle\langle j,\uparrow| + |j,\downarrow\rangle\langle j,\downarrow|) \\ &-h_{j+1}(|j,\uparrow\rangle\langle j+1,\uparrow| - |j,\downarrow\rangle\langle j+1,\downarrow| \\ &+\text{H.c.})], \end{aligned} \tag{B1}$$

where $h_j = h + (\mu - 1)h\delta_{j,N}$. $H_{\text{eff}}$ can be solved numerically. The energy levels of the lowest $2N$ energy states in the TEK and KBS phases are illustrated in Fig. 9, which shows that the perturbative theory is quite good for small enough $h$.

In the TEK phase, the unique ground state can be analytically worked out as

$$\begin{aligned} \left|E_0^{\text{R}}\right\rangle \approx &\sum_{j=1}^{N-2} [\cos q_1 j + \cos(N-j-1)q_1]|j,\uparrow\rangle \\ &+ \sum_{j=N-1}^{N} \frac{[\cos q_1 + \cos(N-2)q_1]}{2\cos q_1 - \mu}|j,\uparrow\rangle, \end{aligned} \tag{B2}$$

where $q_1 \approx \frac{\pi(1-\mu)}{N(1-\mu)+(1+\mu)}$ for $\mu \leqslant 1$. In the KBS phase, it becomes a KBS with odd parity and is denoted by $|\text{KBS}^{\text{R}}\rangle = |E_0^{\text{R}}\rangle$ with $q_1 \approx i \ln\mu$ for $\mu > 1$. Another KBS with even parity can be worked out as

$$\begin{aligned} |\text{KBS}^{\text{NS}}\rangle \approx &\sum_{j=1}^{N-2} [\sin q_1 j - \sin(N-j-1)q_1]|j,\downarrow\rangle \\ &+ \sum_{j=N-1}^{N} (-1)^j \frac{[\sin q_1 - \sin(N-2)q_1]}{2\cos q_1 + \mu}|j,\downarrow\rangle. \end{aligned} \tag{B3}$$

Equations (13) and (14) are recovered by taking $N \to \infty$. The two KBSs are degenerate.

The longitudinal correlation function of the ground state defined in Eq. (17) can be directly worked out in the framework of perturbative theory. By Eq. (B2), we get

$$C_{j,j+r} \approx (-1)^r F(q_1) G(q_1), \tag{B4}$$

in which

$$F(q_1) = \frac{2\cos^2\left(\frac{N-1}{2}q_1\right)}{\frac{2}{N}\left[\frac{\cos q_1 + \cos(N-2)q_1}{2\cos q_1 - \mu}\right]^2 + \frac{1}{N}\sum_{l=1}^{N-2}[\cos l q_1 + \cos(N-l-1)q_1]^2}, \tag{B5}$$

$$G(q_1) = 1 - 2\frac{r}{N} + \frac{\sin(N-2r-2j)q_1 + \sin N q_1 - \sin(N-2j)q_1}{N\sin q_1}. \tag{B6}$$

Substituting $q_1$ into $F(q_1)$ and $G(q_1)$ and taking $N \to \infty$, we find that

$$F(q_1) \to \begin{cases} 1 & (\mu < 1), \\ \frac{1}{2} & (\mu = 1), \\ \frac{N(\mu^2-1)}{2\mu e^{N\ln\mu}} & (\mu > 1), \end{cases} \tag{B7}$$

$$G(q_1) \to \begin{cases} (1-2\alpha) + \frac{\sin[(1-2\alpha-2\frac{j}{N})\pi] - \sin[(1-2\frac{j}{N})\pi]}{\pi} & (\mu < 1), \\ 2(1-2\alpha) & (\mu = 1), \\ 1 - 2\frac{r}{N} + \frac{2\mu e^{N\ln\mu}}{N(\mu^2-1)}[1 - e^{-2(N-r-j)\ln\mu} + e^{-2(r+j)\ln\mu} + e^{-2(N-j)\ln\mu} - e^{-2j\ln\mu}] & (\mu > 1). \end{cases} \tag{B8}$$

By substituting Eqs. (B7) and (B8) into (B4), we can recover the scaling functions $R^{\text{b/i}}(\alpha)$ as described in the main text. We can also get the approximate impurity correlation length $\xi_{\text{i}} = \frac{1}{2|q_1|} \approx \frac{1}{2\ln\mu}$ for the KBS phase ($\mu > 1$).

## APPENDIX C: DETERMINANT REPRESENTATION OF CORRELATION FUNCTIONS

By using Wick's theorem and Majorana fermions,

$$A_j = f_j^\dagger + f_j, \quad B_j = f_j^\dagger - f_j, \tag{C1}$$

the two-site longitudinal correlation function defined in Eq. (17) can be represented by a $r$th-order determinant. First, we can write down

$$C_{j,j+r} = \langle 0^{\text{R}}|\eta_{z_1} B_j A_{j+1} B_{j+1} A_{j+2} \cdots A_{j+r-1} B_{j+r-1} A_{j+r} \eta_{z_1}^\dagger |0^{\text{R}}\rangle. \tag{C2}$$

Then by the contractions

$$\begin{aligned}\langle \eta_{z_1}\eta_{z_1}^{\dagger}\rangle &= 1,\\ \langle A_i A_j\rangle &= -\langle B_i B_j\rangle = \delta_{i,j},\\ \langle B_j A_{j+r}\rangle &\equiv G_{j,j+r} = \sum_q (h_{q,j}-g_{q,j})(h_{q,j+r}+g_{q,j+r}),\\ \langle \eta_{z_1}A_{j+r}\rangle\langle B_j\eta_{z_1}^{\dagger}\rangle - \langle \eta_{z_1}B_j\rangle\langle A_{j+r}\eta_{z_1}^{\dagger}\rangle &\equiv F_{j,j+r} = 2\big(h_{z_1,j}-g_{z_1,j}\big)(h_{z_1,j+r}+g_{z_1,j+r})\end{aligned} \tag{C3}$$

we can arrive at

$$C_{j,j+r} = \det\begin{bmatrix} G_{j,j+1}-F_{j,j+1} & G_{j,j+2}-F_{j,j+2} & \cdots & G_{j,j+r}-F_{j,j+r}\\ G_{j+1,j+1}-F_{j+1,j+1} & G_{j+1,j+2}-F_{j+1,j+2} & \cdots & G_{j+1,j+r}-F_{j+1,j+r}\\ & \vdots & & \\ G_{j+r-1,j+1}-F_{j+r-1,j+1} & G_{j+r-1,j+2}-F_{j+r-1,j+2} & \cdots & G_{j+r-1,j+r}-F_{j+r-1,j+r}\end{bmatrix}. \tag{C4}$$

Except for the translationally symmetric case ($\mu = 1$), this determinant is generally not a Toeplitz determinant due to the presence of impurity ($\mu \neq 1$); however, it can still be evaluated numerically for quite large systems.

The three-site correlation function defined in Eq. (38) can also be represented by a determinant. By Wick's theorem, we have

$$T_{j,j+r,N} = -\langle 0^{\mathrm{R}}|\eta_{z_1}B_N A_N B_j A_{j+1}B_{j+1}A_{j+2}\cdots A_{j+r-1}B_{j+r-1}A_{j+r}\eta_{z_1}^{\dagger}|0^{\mathrm{R}}\rangle. \tag{C5}$$

Then we can write it into a $(r+1)$-th order determinant,

$$T_{j,j+r,N} = -\det\begin{bmatrix} G_{N,N}-F_{N,N} & G_{N,j+1}-F_{N,j+1} & \cdots & G_{N,j+r}-F_{N,j+r}\\ G_{j,N}-F_{j,N} & G_{j,j+1}-F_{j,j+1} & \cdots & G_{j,j+r}-F_{j,j+r}\\ G_{j+1,N}-F_{j+1,N} & G_{j+1,j+1}-F_{j+1,j+1} & \cdots & G_{j+1,j+r}-F_{j+1,j+r}\\ & \vdots & & \\ G_{j+r-1,N}-F_{j+r-1,N} & G_{j+r-1,j+1}-F_{j+r-1,j+1} & \cdots & G_{j+r-1,j+r}-F_{j+r-1,j+r}\end{bmatrix}. \tag{C6}$$

.


[1] S. Sachdev, *Quantum Phase Transitions*, 2nd ed. (Cambridge University Press, Cambridge, 2011).

[2] I. Affleck, in *Exact Methods in Low-dimensional Statistical Physics and Quantum Computing*, edited by J. Jacobsen, S. Ouvry, V. Pasquier, D. Serban, and L. Cugliandolo (Oxford University Press, Oxford, 2010).

[3] S. Lorenzo, T. J. G. Apollaro, A. Sindona, and F. Plastina, Quantum-state transfer via resonant tunneling through local-field-induced barriers, Phys. Rev. A **87**, 042313 (2013).

[4] S. Lorenzo, T. J. G. Apollaro, S. Paganelli, G. M. Palma, and F. Plastina, Transfer of arbitrary two-qubit states via a spin chain, Phys. Rev. A **91**, 042321 (2015).

[5] D.-J. Choi, N. Lorente, J. Wiebe, K. von Bergmann, A. F. Otte, and A. J. Heinrich, Colloquium: Atomic spin chains on surfaces, Rev. Mod. Phys. **91**, 041001 (2019).

[6] H. T. Diep, *Frustrated Spin Systems* (World Scientific, Singapore, 2005).

[7] R. Z. Bariev, Effect of linear defects on the local magnetization of a plane ising lattice, Zh. Eksp. Teor. Fiz. **77**, 1217 (1979) [Sov. Phys. JETP **50**, 613 (1979)].

[8] G. G. Cabrera and R. Jullien, Universality of Finite-Size Scaling: Role of the Boundary Conditions, Phys. Rev. Lett. **57**, 393 (1986).

[9] G. G. Cabrera and R. Jullien, Role of boundary conditions in the finite-size Ising model, Phys. Rev. B **35**, 7062 (1987).

[10] F. Iglói, I. Peschel, and L. Turban, Inhomogeneous systems with unusual critical behaviour, Adv. Phys. **42**, 683 (1993).

[11] M. Campostrini, A. Pelissetto, and E. Vicari, Quantum transitions driven by one-bond defects in quantum Ising rings, Phys. Rev. E **91**, 042123 (2015).

[12] J.-J. Dong, P. Li, and Q.-H. Chen, The a-cycle problem for transverse Ising ring, J. Stat. Mech. (2016) 113102.

[13] J.-J. Dong, Z.-Y. Zheng, and P. Li, Rigorous proof for the nonlocal correlation function in the transverse Ising model with ring frustration, Phys. Rev. E **97**, 012133 (2018).

[14] P. Li and Y. He, Ring frustration and factorizable correlation functions of critical spin rings, Phys. Rev. E **99**, 032135 (2019).

[15] S. M. Giampaolo, F. B. Ramos, and F. Franchini, The frustration of being odd: Universal area law violation in local systems, J. Phys. Commun. **3**, 081001 (2019).

[16] Z.-Y. Zheng, H.-C. Kou, and P. Li, Quaternary Jordan-Wigner mapping and topological extended-kink phase in the interacting Kitaev ring, Phys. Rev. B **100**, 235127 (2019).

[17] Z.-C. Gu and X.-G. Wen, Tensor-entanglement-filtering renormalization approach and symmetry-protected topological order, Phys. Rev. B **80**, 155131 (2009).

[18] B. Zeng, X. Chen, D.-L. Zhou, and X.-G. Wen, *Quantum Information Meets Quantum Matter: From Quantum Entanglement to Topological Phase in Many-Body Systems* (Springer, New York, 2019).

[19] G. Torre, V. Marić, F. Franchini, and S. M. Giampaolo, Phys. Rev. B **103**, 014429 (2021).

[20] G. Francica, T. J. G. Apollaro, N. Lo Gullo, and F. Plastina, Local quench, Majorana zero modes, and disturbance propagation in the Ising chain, Phys. Rev. B **94**, 245103 (2016).

[21] T. J. G. Apollaro, G. Francica, D. Giuliano, G. Falcone, G. M. Palma, and F. Plastina, Universal scaling for the quantum Ising chain with a classical impurity, Phys. Rev. B **96**, 155145 (2017).

[22] It is noteworthy that the redundant degrees of freedom in $H^{\mathrm{R}}$ and $H^{\mathrm{NS}}$ compose another quantum Ising ring with APBC, $\tilde{H} = P_z^+ H^{\mathrm{R}} + P_z^- H^{\mathrm{NS}}$. So the four relevant Hamiltonians are linked together by a complete *quaternary Jordan-Wigner mapping* as uncovered in Ref. [16].

[23] E. Lieb, T. Schultz, and D. Mattis, Two soluble models of an antiferromagnetic chain, Ann. Phys. **16**, 407 (1961).

[24] F. Iglói and J. Zittartz, Quantum Ising model with staggered interaction, Z. Phys. B Condens. Matter **70**, 387 (1988).

[25] C.-K. Chiu, J. C. Y. Teo, A. P. Schnyder, and S. Ryu, Classification of topological quantum matter with symmetries, Rev. Mod. Phys. **88**, 035005 (2016).

[26] M. Tang and Y. He, Nonlocal behaviors of spin correlations in the Haldane-Shastry model, Phys. Lett. A **384**, 126043 (2020).

[27] First, this assumption is supported by the perturbative theory (Appendix B), which gives $C^{\mathrm{b}}(r,\alpha) = (-1)^r R^{\mathrm{b}}(\alpha)$. Second, the missing part $C^{\mathrm{b}}(r)$ is recovered by rigorous numerical calculation.

[28] G. Vidal, J. I. Latorre, E. Rico, and A. Kitaev, Entanglement in Quantum Critical Phenomena, Phys. Rev. Lett. **90**, 227902 (2003).

[29] T. Hirano and Y. Hatsugai, Entanglement entropy of one-dimensional gapped spin chains, J. Phys. Soc. Jpn. **76**, 074603 (2007).

[30] C. N. Yang, The spontaneous magnetization of a two-dimensional Ising model, Phys. Rev. **85**, 808 (1952).

[31] P. D. Francesco, P. Mathieu, and D. Sénéchal, *Conformal Field Theory* (Springer, New York, 2012).

[32] A. Milsted and G. Vidal, Extraction of conformal data in critical quantum spin chains using the Koo-Saleur formula, Phys. Rev. B **96**, 245105 (2017).

[33] Y. Zou, A. Milsted, and G. Vidal, Conformal Data and Renormalization Group Flow in Critical Quantum Spin Chains Using Periodic Uniform Matrix Product States, Phys. Rev. Lett. **121**, 230402 (2018).

[34] Y. Zou, A. Milsted, and G. Vidal, Conformal Fields and Operator Product Expansion in Critical Quantum Spin Chains, Phys. Rev. Lett. **124**, 040604 (2020).

[35] Y. Zou and G. Vidal, Emergence of conformal symmetry in quantum spin chains: Antiperiodic boundary conditions and supersymmetry, Phys. Rev. B **101**, 045132 (2020).

[36] H. Labuhn, D. Barredo, S. Ravets, S. de Léséleuc, T. Macrì, T. Lahaye, and A. Browaeys, Tunable two-dimensional arrays of single Rydberg atoms for realizing quantum Ising models, Nature (London) **534**, 667 (2016).

[37] Y. Wang, J. Gao, X.-L. Pang, Z.-Q. Jiao, H. Tang, Y. Chen, L.-F. Qiao, Z.-W. Gao, J.-P. Dou, A.-L. Yang, and X.-M. Jin, Parity-Induced Thermalization Gap in Disordered Ring Lattices, Phys. Rev. Lett. **122**, 013903 (2019).

[38] T. Scaffidi, D. E. Parker, and R. Vasseur, Gapless Symmetry-Protected Topological Order, Phys. Rev. X **7**, 041048 (2017).

[39] P. Pfeuty, The one-dimensional ising model with a transverse field, Ann. Phys. (NY) **57**, 79 (1970).